■ 1110

Rain attenuation statistics for mobile satellite communications estimated from radar measurements in Malaysia

Mohammad Ibrahiem Abozeed[1], Manhal Alhilali[2], Lam Hong Yin[3], Jafri Din[*4]
[1,2,4]Wireless Communication Centre, Faculty of Electrical Engineering, Universiti Teknologi Malaysia,
81310 Johor Bahru, Johor, Malaysia
[3]Department of Electrical Engineering Technology, Faculty of Engineering Technology,
Universiti Tun Hussein Onn Malaysia, Pagoh, 86400 Johor, Malaysia
*Corresponding author, e-mail: jafri@utm.my

Abstract

Mobile satellite communications will play a significant role in the next 5th generation mobile services. The use of high-frequency bands will be the enabler of this advancement. However, at high frequencies, excess rain attenuation causes severe signal losses and presents a major threat for the system availability, especially in the tropical region. To that end, this study presents the rain attenuation impact on mobile satellite communications estimated using long-term radar measurements in Malaysia, by exploiting the horizontal structure of rain from the radar database and simulating inner-city and highway mobile terminals scenarios. Additionally, a scaling factor was presented to scale available fixed satellite terminals measurements to mobile terminals operating at the same locality under similar conditions. In comparison to the available link measurements, the radar database was reliable enough to provide highly accurate estimates. In all simulation scenarios, the mobile terminal will depart the rainy area soon enough and experience lower attenuation statistics in comparison with the fixed terminal. The provided results will help determine the overall future system performance, especially in tropical regions.

Keywords: mobile satellite communication, radar, rain attenuation, tropical region

1. Introduction

The future mobile satellite systems will provide some major changes to the current systems. It will be designed to deliver higher capacity with the use of higher frequency bands [1, 2], as satellite communications will play a central role towards achieving the next 5th generation (5G) mobile communication requirements [3, 4]. At high frequencies, the excess rain attenuation is a huge setback, especially in tropical regions where higher rain rates are expected [5–7]. This also provide a challenging task for system designers when higher availability requirements is provided. Long-term rain attenuation statistics are required to provide a better understanding for mobile terminals, which is different form the fixed terminals statistics due to the movement involved [8]. Other implications added to the mobile satellite systems such as shadowing, and multipath [9] in addition to the rain attenuation, can render the system unusable. This article will only discuss the rain attenuation, as the recent advancement in research on smart antenna and antenna arrays [10, 11] will reduce these multipath effects. However, rain will remain the biggest challenge, especially in tropical regions such as Malaysia [12, 13].

In this work the cumulative probability distribution exceeded at a given rain attenuation A (dB) in a fixed satellite system $P_F(A)$ is transformed into that applicable to a satellite system for mobile terminals $P_M(A)$ operating in the same geographical region, carrier frequency and weather conditions, as suggested by [14]. The provided result should allow the transformation to be applied for similar systems operating in tropical regions. Keeping in mind that a complete channel model will require the inclusion of multipath and shadowing effects. As suggested by [14], two models for the mobile terminals are presented, which are inner-city (zigzag-roads, ring-roads) and highways (straight-roads) with the mobile terminal speed modelled as log-normal random variable. Radar rain-rate maps was used, from Kluang meteorological radar located in Johor, Malaysia. With database collected from January 2007 to December 2008 of

continuous operation. This database is long enough to produce reliable statistics as shown later. City streets are applied on the rain-maps by plotting a grid of square cells and straight lines to analyse the previously mentioned scenarios. And a mobile terminal operating at 12 GHz with radio link toward the geostationary MEASAT located at $91.5°$ W was simulated, which is similar to the recorded fixed terminal at Kuala Lumpur [15].

The result reported in this article, shows that both fixed system and mobile systems can be compared very well. The attenuation experienced by the mobile system is less than fixed system as reported in [14]. However, different factors and higher attenuation resulted in tropical regions due to the localized climate, and the nature of rain. This article is organized as follow: section 2 present the study database, followed by rain attenuation calculation in section 3 for both fixed systems as well as mobile systems. Section 4 present the simulation results for inner-city speeds, while section 5 present it for highway speeds. Section 6 examine the effects of different elevation angles, and finally, section 7 delivers some conclusions.

2. Radar Database

The Kluang radar has 4.3-m parabolic reflector (38.4 dB gain). 64 consecutive echoes are averaged for the computation of the reflectivity factor Z with error of ± 0.8 dB. The minimum detectable signal is -110 dBm. The maximum range of operation is about 250 km, however, the used database was collected only up to 50 km.

The database used in this study is for the period from January 2007 to December 2008 with a continuous operation of the radar. Every 10 minutes the radar perform a complete volumetric scan with 15 elevation angles (0.5°, 0.8°, 1.1°, 1.4°, 1.9°, 2.5°, 3.3°, 4.4°, 5.8°, 7.7°, 10.3°, 13.6°, 18.1°, 24.1° and 32.1°). Five of these scans were used to obtain pseudo constant altitude plan position indicator (CAPPI) namely 1.4°,1.9°,2.5°,3.3° and 4.4° at a constant plane of 1.5 km from ground as sketched in Figure 1. Each CAPPI image generated from the total scanned time of 90 seconds, which help to obtain the best spatial resolution with instant image of rain.
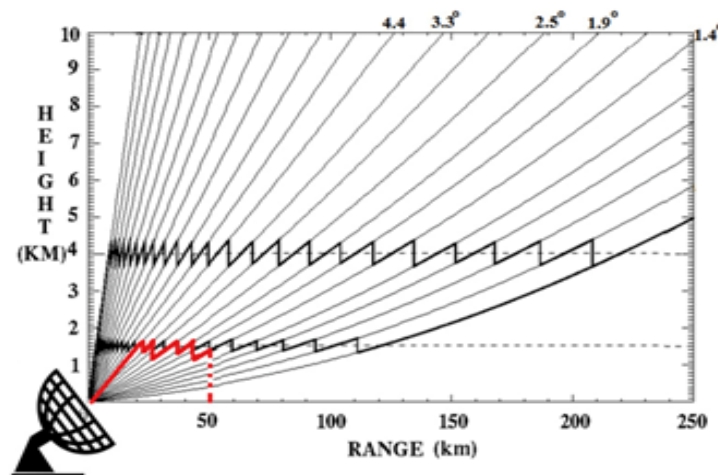

Figure 1. Five azimuth scans with elevation angles of 1.4°, 1.9°, 2.5°, 3.3° and 4.4°, combined to obtain CAPPI at 1.5 km of height

The rain rate R then computed from the measured radar reflectivity Z using the following Z-R relation

$$Z = 300\, R^{1.4} \tag{1}$$

where Z in mm⁶m⁻³ and R in mm/h, the coefficients 300 and 1.4 have been derived from the Malaysian raindrop size distribution (DSD) measurement by [16], instead of the commonly used

Marshall-Palmer DSD relationship [17] with the coefficient of 200 and 1.6, which were found not able to represent tropical climate [18].

The probability matching method [19] was employed to influence the reflectivity Z to represent the reflectivity converted from the long-term statistic of rain-rate measurement made available by the Malaysian Department of Irrigation and Drainage [19]. After the modification of reflectivity values, the database consists only of 11 reflectivity levels which correspond to quite a coarse quantization of the rainfall intensity. The minimum observable rain rate was 0.2 mm/h.

The static clutter map technique [20]. Is then used to account for the ground clutter and blockage. Then the database which is initially in polar coordinates, is converted to 40000 cartesian cells of side 500 m, with total square area of side 100 km. with sides parallel to the north-south (N-S) and east-west (E-W) directions. More details on data acquisition and processing can be found in [16]. For the present study, the inner cells affected partially by clutter, assigned values of the surrounding cells with valid data to maintain as much as possible the continuous horizontal extent of rain. This technique was also adopted for the blind area around the radar site. Following this process, the remaining number of useful cells amounts to 32440 representing an area of 8110 km². And the total database consists of 42234 maps.

2.1. Rain Attenuation Calculation

After obtaining the horizontal structure of rain using the radar maps, the vertical structure needs to be modelled in order to compute the slant path rain attenuation. Considering all the atmospheric layers defined in [21]. Starting from the ground, layer A where hydrometeors in the form of raindrops, with water temperature of 20° C, and the rain rate obtained from radar maps. The melting layer B is then simulated where water temperature at 0° C, and the rain rate R_a is related to the first layer rain rate R by the relation $R_a = 3.134\,R$ [21].

The precipitation height H_R above sea level containing both layers is defined following the International Telecommunications Union (ITU) recommendation [22], which is 4969 m for the radar location, yielding of average precipitation height $H = 4969 - 255 = 4714$ m. Then the melting layer B depth is assumed to be 400 m at any altitude [21], so that $4714 - 400 = 4314$ m. Both layers are used for all the maps regardless of rain types. This assumption was found [14,21], to give enough resolution and minimum error for the comparison between fixed and mobile systems.

Rain attenuation A(dB) is calculated as a line integral of the specific rain attenuation $\gamma = kR^\alpha$ [23], with the values of rain rate found in the cells sampled by the projection at ground of the slant path, and to the layer:

$$A = \int_0^{L_A} \gamma_A(x)\,dx + \int_{L_A}^{L_B} \gamma_B(x)\,dx \tag{2}$$

where x is slant coordinate (at elevation angle θ), L_A is slant length in layer A, L_B is slant length in layer B, and $\gamma_A(x)$, $\gamma_B(x)$ are the specific rain attenuations in layer A and B, given by:

$$\gamma_A(x) = k\,R^\alpha(x), \gamma_B(x) = k\,R_a{}^\alpha(x) = k\left(3.134R(x)\right)^\alpha \tag{3}$$

where k and α are parameters given by the ITU-R [23] as a function of frequency and polarization, at 12 GHz, $k = 0.02455$, $\alpha = 1.1617$. knowing that both parameters can change significantly with different raindrop size distributions, and hydrometer temperature, however, this is not the concern of this study.

The value of rain attenuation A is similar of both fixed and moving terminals but with different time durations as suggested in [14]. For that, the value A was calculated only once at the centre of each radar cell, to force both type of terminals to measure the exact value, and the value would not change for the mobile terminal moving inside the same cell, the only change between the two terminals was in the duration and the rate of change in motion. Considering the slant path to the satellite MEASAT, with elevation angle $\theta = 76°$. The number of useful cells need to be reduced to remove the cells where it is not possible to incorporate the specific attenuation for the entire path, to guarantee that both fixed and mobile terminals are always able to measure attenuation for the complete slant path. For the 76° slant path, $L_B = 4714/\sin(76) = 4999$ m and its projection at ground $L_g = 4999\cos(76) = 1209.4$ m. Beside that other elevations angles are simulated in this study with $30°, 45°, 60°$ and $90°$, and by

calculating the useful cells for each path, the number varies from 37875 ($\theta = 30°$) to all the cells 42234 ($\theta = 90°$). To keep the comparison fair for each angle, the same 37875 cells were considered for all the values of θ. The simulated fixed system results, operation at Ku band at 12 GHz, is then tested against beacon experimental data collected at Kuala Lumpur to the satellite MEASAT-1 in the year August 1996 to July 1997 [15]. Additionally, a simulation at Ka band at 20 GHz is done and tested against the data collected in Johor, to the satellite Syracuse 3A with elevation angle of $25°$, in the period 2015-2016 as reported in [24]. Figure 2 reports the cumulative probability distributions $P_F(A)$ that the rain attenuation A (dB) is exceeded for both links in an average year, and the predicated by the radar simulations.

Both simulated and measured curves were in very good agreement regardless of the observation period, the radar produced a very reliable of the long-term $P_F(A)$ by sampling 37875 slant paths. Which will also be the case to the long-term $P_M(A)$ of the mobile terminals in the following sections.
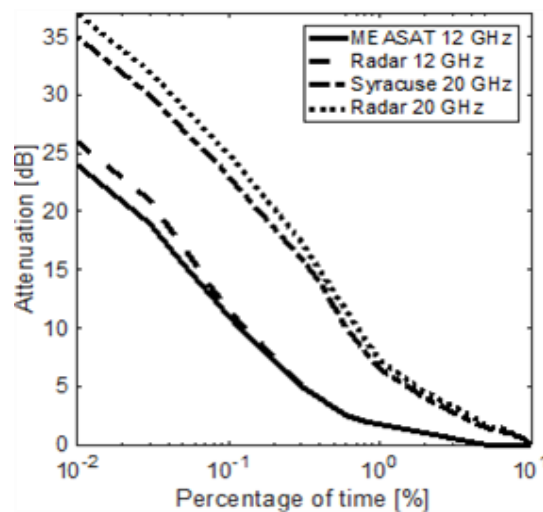

Figure 2. $P_F(A)$ (%) the rain the rain attenuation A (dB) is exceeded for both beacon receiver's measurement [10, 19] and predicted by radar simulation

2.2. Inner City Mobile Terminals

As a simplification the city block grid was assumed to have square side of $d = 500$ m, similar to the radar cells, the streets intersection designed to be within the centre of the radar cell, where the fixed terminal was placed, the mobile terminal was then driven with constant speed v for all the cell distance d, with a log-normal probability with median value of $M = 30$ km/h, or $M = 60$ km/h, with maximum allowed values of 70 and 110 km/h, respectively. These two distribution models are labelled as M1, M2 to represent low and fast speed, representing the average distribution of inner-city speeds in Malaysia. No speed change was considered for the purpose this study.

At each intersection the mobile terminal could change direction with equal probability $p_{right} = p_{left} = (1 - p_{straight})/2$, so that $p_{straight} + p_{left} + p_{right} = 1$, these conditions were used for the zigzag road, while square ring-roads are detailed later. A mobile terminal was no longer considered as it left the map or there were no more radar maps for the rain storm. The results provided here are averaged over 37875 fixed terminals, 100 terminals for zigzag-roads, and 20 terminals for ring-roads.

Figure 3 shows probability distributions exceeded in the mobile systems $P_M(A)$ with M1, compared to the cumulative probability that the same value of A is exceeded in the fixed system $P_F(A)$, averaged over the 37875 cells of the useful area. It is observable that for all values of A, $P_M(A) < P_F(A)$. Additionally, the higher the probability of the mobile terminal going in a straight line $p_{straight} > 0.5$, the smaller the value of $P_M(A)$. Figure 4 shows $P_M(A)$ for mobile terminals moving with M2, lower attenuation observed since the terminals will leave the area faster due to

the higher speed. The Figures 3, 4, clearly demonstrate the possibility to scale any value of $P_M(A)$ from $P_F(A)$, as described by [14], following the equation:

$$P_M(A) = \xi\, P_F(A) \tag{4}$$

while the probability scaling factor ξ was verified to be independent of attenuation by [14], the factor is still dependent on the spatial horizontal distribution of rain, rain types, and the properties of the climatic region.
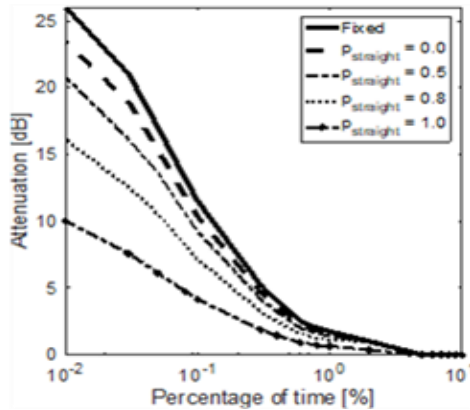

Figure 3. $P_M(A)$ the rain attenuation A (dB) is exceeded for mobile system M1 versus the fixed system $P_F(A)$, $p_{straight} = 0.0, 0.5, 0.8, 1, d = 500$ m
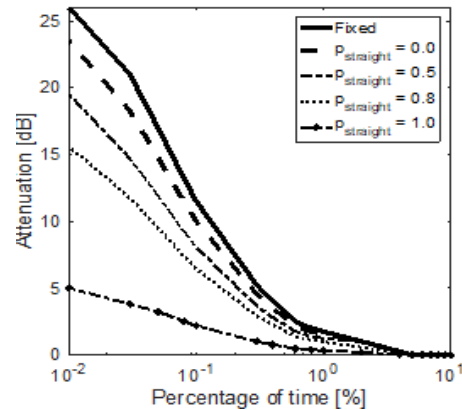
Figure 4. $P_M(A)$ the rain attenuation A (dB) is exceeded for mobile system M2 versus the fixed system $P_F(A)$, $p_{straight} = 0.0, 0.5, 0.8, 1, d = 500$ m

Thus, it is possible to calculate $P_M(A)$ simply by scaling $P_F(A)$ using the constant factor ξ. However, this factor should be analysed for each climatic region. Note that, this factor is independent of frequency, making it very effective to be used for any different link frequency. Table 1 shows the computed values of ξ for this study representing tropical regions, in comparison with the values obtained by [14], which can be used for temperate regions.

Table 1. The Scaling factor ξ for M1 and M2 for Tropical Region, Versus Values Obtained by [14] for Temperate Regions.

$p_{straight}$	M1 Tropical	M1 [14]	M2 Tropical	M2 [14]
0.5	0.8	0.72	0.7	0.59
0.8	0.62	0.5	0.56	0.42
1	0.36	0.16	0.19	0.07

In case the dimension of the streets D changed, the mobile terminal will continue in straight line for longer time before changing its direction. By simulating the street grid with longer dimension where $D = 1000, 2000$ m, the mobile terminal left the rainy area sooner than before, and therefore, receive less attenuation. Table 2 shows the value of ξ for both models M1, M2, where smaller values of ξ indicates lower attenuation.

To simulate the ring-roads square rings plotted around the radar location with different side lengths was used, and the mobile terminal moved in two directions (clockwise, counter clockwise). The ring-roads usually used to represent buses and trains. The results obtained for each ring-road are shown in Figure 5. All mobile terminals received $P_M(A)$ similar to the fixed terminal $P_F(A)$, showing no significant difference between fixed and mobile terminals.

Table 2. The Scaling Factor ξ for M1 and M2, as a Function of Street Dimension
D=500, 1000, 2000 m

	M1			M2		
$p_{straight}$	500	1000	2000	500	1000	2000
0.5	0.8	0.69	0.66	0.7	0.59	0.56
0.8	0.62	0.6	0.49	0.56	0.54	0.43
1	0.36	0.35	0.36	0.19	0.18	0.17
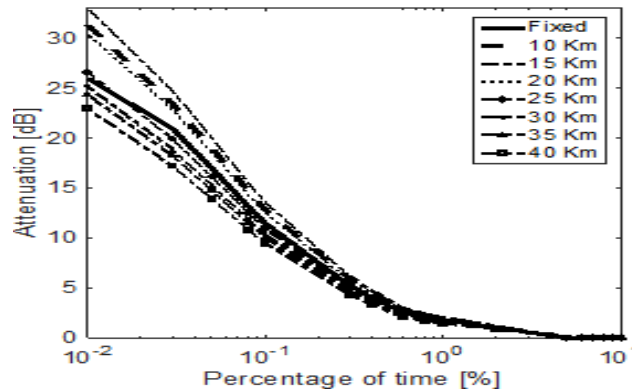
Figure 5. $P_M(A)$ (%) the rain attenuation A (dB) is exceeded for mobile system moving in ring-roads versus the fixed system $P_F(A)$. Side length of the square ring roads = 10, 15, 20, 25, 30, 40 km

2.3. Highway Mobile Terminals

To simulate the Highway traffic in Malaysia, a mobile terminal was driven across the radar area in straight line from different directions, with log-normal distribution of speeds with median value of 90 km/h, and maximum limit of 120 Km/h. This distribution model was labelled (M3) to represent highway traffic. The directions simulated are east-west (EW), west-east (WE), north-south (NS), and south-north (SN). Figure 6 shows the $P_M(A)$ for mobile terminals moving in straight lines as described in M3, very low attenuation observed since the terminals will leave the area faster due to the higher speed. Knowing that not all mobile terminals will be moving at the same speeds in M3, in case of a traffic. Figure 7 shows a comparison of the average attenuation between terminals moving in high speeds as in M3, and lower speed as in M1 however only locked in straight lines. It is obvious that the scaling factor ξ will be affected by the terminal speed as it will leave the rainy area sooner in case of higher speed movement.
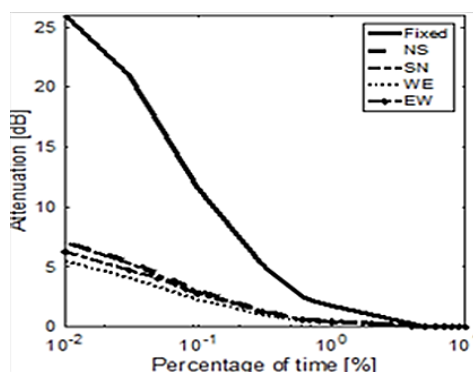

Figure 6. $P_M(A)$ the rain attenuation A (dB) is exceeded for mobile system moving in highway speeds in straight lines as described in M3 versus the fixed system
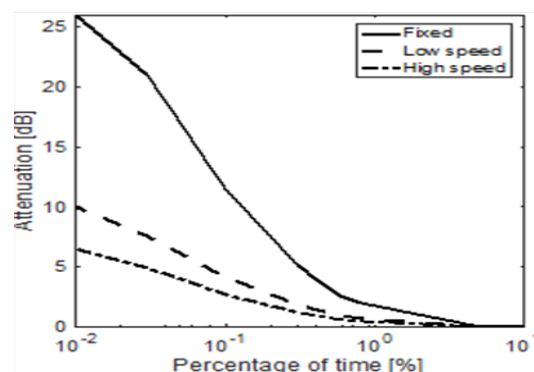

Figure 7. $P_M(A)$ (%) the rain attenuation A (dB) is exceeded for mobile system moving in straight lines averaged in all directions for M1 and M3 versus the fixed system $P_F(A)$

3. Impact of Link Elevation Angles

In case different elevation angles were utilized, this is expected in the future use of satellite communications [25]. The fixed link performance was simulated for the values of $\theta = 30°, 45°, 60°, 90°$ in similar vertical plane as MEASAT slant-path. Figure 8 present $P_F(A, \theta)$ average d over the 37875 cells. As anticipated $P_F(A)$ increases as θ decreases. The new attenuation value $A(\theta)$ can be simply scaled from known attenuation value $A(\theta_0)$ following the relation $\frac{A(\theta)}{A(\theta_0)} = \frac{\sin\theta_0}{\sin\theta}$, where in our case $\theta_0 = 76°$.
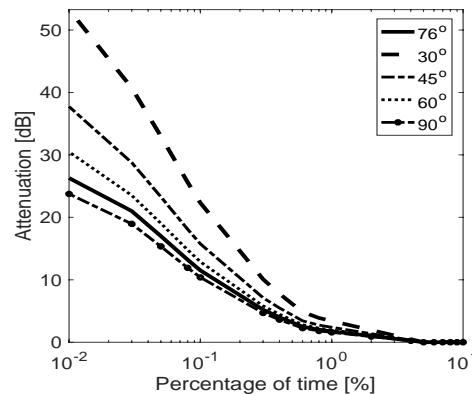

Figure 8. $P_F(A)$ (%) the rain attenuation A (dB) is exceeded for fixed systems as a function of elevation angle, averaged over the 37875 cells

Mobile terminals were also simulated to examine the change of the factor $\xi(\theta)$. No large changes were observed. For that it is safe to assume that the scaling factor is independent of elevation angle, and only by scaling the fixed terminal attenuation statistics to the new elevation angle, we can then use the same factor to obtain the attenuation for mobile systems.

4. Conclusion

The cumulative probability distributions $P_F(A)$, and a given rain attenuation A (dB) for fixed satellite systems, were examined and scaled to the probability of the mobile satellite systems $P_M(A)$. Different scenarios were investigated for the mobile system by simulating the inner-city transportation as well as for highway speeds. It was found that the mobile system will experience less attenuation in comparison to the fixed system for all scenarios except for ring-roads, where similar attenuation level is expected. The highway speed terminals received the lowest rain attenuation, followed by inner city traffic with higher probability of going in straight line. In both cases the mobile terminal will depart the rainy area sooner which result in lower attenuation statistics. Additionally, the scaling factor ξ for different speeds, and probability of directions was presented and tabulated. Finally, as mobile satellite systems are also affected by shadowing and multipath, only rain attenuation was examined in this study, where the advancement in the satellite antenna design are expected to overcome these extra issues and only rain attenuation will determine the system performance, especially in tropical regions.

Acknowledgment

References
[1]   Siles GA, Riera JM, Garcia-del-Pino P. Atmospheric attenuation in wireless communication systems at millimeter and THz frequencies [Wireless Corner]. *IEEE Antennas Propag Mag.* 2015; 57(1): 48–61.

[2] O'Hara JF, Grischkowsky DR. *Terahertz atmospheric propagation studies in support of wireless remote sensing*. In: ProcSPIE. 2018. Available from: https://doi.org/10.1117/12.2305019

[3] Jia M, Gu X, Guo Q, Xiang W, Zhang N. Broadband Hybrid Satellite-Terrestrial Communication Systems Based on Cognitive Radio toward 5G. *IEEE Wirel Commun*. 2016; 23(6): 96–106.

[4] Cui X, Gulliver TA, Li J, Zhang H. Vehicle positioning using 5G millimeter-wave systems. *IEEE Access*. 2016;

[5] Alhilali M, Din J, Schönhuber M, Lam HY. Estimation of Millimeter Wave Attenuation Due to Rain Using 2D Video Distrometer Data in Malaysia. *Indones J Electr Eng Comput Sci*. 2017; 7(1): 164–169.

[6] Jong SL, Riva C, D'Amico M, Lam HY, Yunus MM, Din J. Performance of synthetic storm technique in estimating fade dynamics in equatorial M alaysia. *Int J Satell Commun Netw*. 2018.

[7] Alhilali M, Lam HY, Din J. Comparison of Raindrop Size Distribution Characteristics across the Southeast Asia Region. *TELKOMNIKA Telecommunication Computing Electronics and Control*. 2018; 16(6): 2522–2527.

[8] Ferreira PVR, Paffenroth R, Wyglinski AM. Interactive Multiple Model Filter for Land-Mobile Satellite Communications at Ka-Band. *IEEE Access*. 2017; 5: 15414–15427.

[9] Fontán FP, Vázquez-Castro M, Cabado CE, García JP, Kubista E. Statistical modeling of the LMS channel. *IEEE Trans Veh Technol*. 2001;

[10] Luo Q, Gao S, Sumantyo JTS. Smart antennas for mobile satellite communications. In: Antennas and Propagation (APCAP), 2014 3rd Asia-Pacific Conference on. IEEE; 2014: 104–107.

[11] An K, Liang T, Yan X, Li Y, Qiao X. Power Allocation in Land Mobile Satellite Systems: An Energy-Efficient Perspective. *IEEE Commun Lett*. 2018; 22(7): 1374–1377.

[12] Lam HY, Luini L, Din J, Alhilali MJ, Jong SL, Cuervo F. Impact of Rain Attenuation on 5G Millimeter Wave Communication Systems in Equatorial Malaysia Investigated Through Disdrometer Data. In: 11th European Conference on Antennas and Propagation (EUCAP). Paris: IEEE; 2017: 1802–1806.

[13] Li N, Wang Z, Chen X, Austin G. Studies of General Precipitation Features with TRMM PR Data: An Extensive Overview. *Remote Sens*. 2019; 11(1): 80.

[14] Matricciani E. Experimental Rain Attenuation Statistics Estimated from Radar Measurements Useful to Design Satellite Communication Systems for Mobile Terminals. *IEEE Trans Veh Technol*. 2000; 49(5): 1534–1546.

[15] Ismail AF, Watson PA. Characteristics of fading and fade countermeasures on a satellite-Earth link operating in an equatorial climate, with reference to broadcast applications. *IEE Proceedings-Microwaves, Antennas Propag*. 2000; 147(5): 369–373.

[16] Lam HY, Din J, Jong SL. Interpretation procedure of meteorological radar data for propagation application in heavy rain region. *ISAP 2014 - 2014 Int Symp Antennas Propagation, Conf Proc*. 2015; 579–580.

[17] Marshall JS, Palmer WMK. the Distribution of Raindrops With Size. *J Meteorol*. 1948;5(4):165–166.

[18] Lam HY, Luini L, Din J, Capsoni C, Panagopoulos AD. Preliminary investigation of rain cells in equatorial Malaysia for propagation applications. *RFM 2013-2013 IEEE Int RF Microw Conf Proc*. 2013; 243–246.

[19] Calheiros R V, Zawadzki I. Reflectivity-rain rate relationships for radar hydrology in Brazil. *J Clim Appl Meteorol*. 1987; 26(1): 118–132.

[20] Gabella M, Notarpietro R. *Ground clutter characterization and elimination in mountainous terrain*. In: Proceedings of ERAD. 2002.

[21] Matricciani E. Rain attenuation predicted with a two-layer rain model. *Eur Trans Telecommun*. 1991; 2(6): 715–727.

[22] ITU-R. Rain Height Model for Prediction Methods. *Rec ITU-R P839-4*. 2013;4:1–3.

[23] ITU. P. 838-3 Specific attenuation model for rain for use in prediction methods. ITU-R Recommendations, P Series Fasicle. Geneva, Switzerland: ITU; 2005: 1–5.

[24] Cuervo F, Lam HY, Din J Bin, Castro JR, Schmidt M, Schonhuber M. *The JOANNEUM RESEARCH SatCom Ka and Q band campaigns in Europe and Malaysia*. 2017 11th Eur Conf Antennas Propagation, EUCAP 2017. 2017; (October 2013): 1476–1480.

[25] Jong SL, Lam HY, D'Amico M, Cuervo F, Yunus MM, Din J. Impact of Link Elevation Angles on Rain Attenuation Statistics in Heavy Rain Region Predicted Using the Synthetic Storm Technique. *J Telecommun Electron Comput Eng*. 2017; 9(3–8): 17–20.